A novel amplified electrochemiluminescence biosensor based on Au NPs@PDA@CuInZnS QDs nanocomposites for ultrasensitive detection of p53 gene

Yang Liu, Xueqian Chen, Qiang Ma

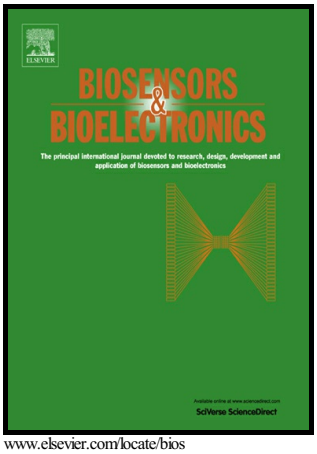

www.elsevier.com/locate/bios

PII: S0956-5663(18)30455-X
DOI: https://doi.org/10.1016/j.bios.2018.06.023
Reference: BIOS10543

To appear in: *Biosensors and Bioelectronic*

Received date: 10 April 2018
Revised date: 29 May 2018
Accepted date: 8 June 2018

Cite this article as: Yang Liu, Xueqian Chen and Qiang Ma, A novel amplified electrochemiluminescence biosensor based on Au NPs@PDA@CuInZnS QDs nanocomposites for ultrasensitive detection of p53 gene, *Biosensors and Bioelectronic,* https://doi.org/10.1016/j.bios.2018.06.023

A novel amplified electrochemiluminescence biosensor based on Au NPs@PDA@CuInZnS QDs nanocomposites for ultrasensitive detection of p53 gene

Yang Liu, Xueqian Chen, Qiang Ma*

Department of Analytical Chemistry, College of Chemistry, Jilin University, Changchun, 130012, China

*Corresponding author. Tel.: +86-431-85168352. E-mail address: *Qma@jlu.edu.cn*

Abstract

In this work, a novel surface plasmon resonance (SPR) enhanced electrochemiluminescence (ECL) biosensing model was first designed based on Au NPs@polydopamine (PDA)@CuInZnS QDs nanocomposite. Au NPs were coated with the PDA layer via the electrostatic force. CuInZnS QDs were bound on the surface of Au NPs@PDA nanocomposite. CuInZnS QDs worked as ECL luminophore in the sensing application. PDA shell not only controlled the separation length between Au NPs and QDs to induce SPR enhanced ECL response, but also limited the potential charge transfer and ECL quenching effect. As a result, the nanocomposite ECL intensity was twice that of QDs with $K_2S_2O_8$. The tumor suppressor p53 gene was detected in the amplified ECL sensing system. The sensing method has a linear response in the range of 0.1 nmol/L to 15 nmol/L with a detection limit of 0.03 nmol/L. The DNA biosensor based on the nanocomposite showed excellent sensitivity, selectivity, reproducibility and stability and was applied in spiked human serum samples with satisfactory results.

Keywords: CuInZnS QDs, polydopamine, surface-enhanced ECL, nanocomposite, biosensor, p53 gene.

1. Introduction

The p53 tumor suppressor gene plays an important role in the protein expression. (Xu et al., 2017) The p53 gene has a specific transcriptional activation, as a human tumor suppressor gene, it has the function of preventing cancer and repairing defects. More than 50% of all malignancies have mutations in the p53 gene. After the mutagenesis of p53 gene, it has changed from a tumor suppressor gene to an oncogene due to the change of its spatial conformation. Therefore, some detection methods have been developed for p53 gene, including ELISA (Tendler et al., 1999), liquid chromatography-tandem mass spectrometry (Jiang et al., 2018), immunohistochemistry (IHC) (Milicevic et al., 2014) etc. Despite these methods exhibit excellent sensitivity and selectivity, time-consuming and sophisticated sample pre-treatment is required. Thus, it is still essential to develop a simple, rapid and accurate method for the determination of p53 gene.

ECL is an ideal analysis method that combines the simplicity of electrochemistry with high sensitivity, low background interference, and wide linear ranges of chemiluminescnce methods. (Liu et al., 2016; Chen et al., 2016) Depending on the reaction process and the substances involved in the reaction, ECL can be divided into two classes, the annihilation ECL and the co-reactant ECL. Since the annihilation ECL is influenced by the stability of intermediate, diffusion rate and voltage windows of solvent, it was always applied in the energy level calculation, valence bond theory and measurement of electrode kinetic parameter. (Zhang et al., 2017) Co-reactant ECL, related to the type and concentration of co-reactants, is widely used in environmental monitoring (Yang et al., 2017), food safety testing (Ye

et al., 2017), and immunoassay. (Khoshfetrat et al., 2018; Wu et al., 2017; Zhang et al., 2017) The most traditional ECL system included tris(2,2′-bipyridine)-ruthenium(II) ($Ru(bpy)_3^{2+}$) as ECL luminophore with tripropylamine (TPA) as co-reactant. And recent years, quantum dots (QDs) has become an ideal ECL luminophore due to their unique properties such as long lifetime, narrow emission peaks, size-tunable emission spectrum, feasibility for surface modification, high photo-bleaching threshold and good chemical stability. (Chen et al., 2014; Wang et al., 2014; Lin et al., 2014)

Although many QDs (e.g. CdTe QDs (Liu et al., 2016) and CdTe@ZnS QDs (Le et al., 2016)) have been used as ECL luminophore, there are still two major limitations of QDs in the ECL application, including the high toxicity from heavy metal elements and the low ECL efficiency. Therefore, the toxic-element-free QDs were employed to resolve the toxic issue of II−VI and III−V QDs. On the other hand, new ECL mechanism and sensing methodology were explored to enhance QDs ECL signal. A significant ECL enhancement was designed with localized SPR of noble metal NPs, which was also called surface-enhanced ECL (SEECL). In the SEECL model, the ECL emission from QDs can induce SPR of Au NPs, and the induced SPR can in turn enhance the ECL response of the QDs. For example, Xu's group has investigated the SEECL based on a separation length of ca. 12 nm between CdS QDs and Au NPs. (Wang et al., 2011) Until now, there are only few reports in the QDs with SEECL research. It was because the noble metal NPs played a special role in both SEECL and ECL resonance energy transfer in one QDs-based ECL sensing system. Meanwhile, most reported QD-based SEECL systems were depended on DNA, which was used to regulate the distance between QDs and Au NPs. So, it is important to develop new QDs-based SEECL sensing system without ECL resonance energy transfer.

In order to overcome the above-mentioned limitations, we try to develop a novel SEECL sensor in this work. The procedure of synthesizing Au NPs@PDA@QDs nanocomposites was shown in Scheme 1. We coated a PDA layer on Au NPs by electrostatic force and bound CuInZnS QDs on the surface of Au NPs@PDA. To our best knowledge, it is the first time to design a SEECL biosensor based Au

NPs@PDA@QDs nanocomposites. The novel ECL biosensor possessed serval advantages: (i) CuInZnS QDs are ideal luminophore for ECL sensing application. Compared with the traditional chalcogenide QDs, CuInZnS QDs have good biocompatibility and non-toxicity. (Chen et al., 2018) Moreover, the luminescence of CuInZnS QDs is mainly due to surface defect state emission. So, the ECL emission of QDs depends on the surface states with high ECL efficiency. (Chen et al., 2017). (ii) Au NPs in the core of the nanocomposite worked as ECL enhancer. Au NPs had a high extinction coefficient, broad absorption spectrum, and surface plasmon resonance. (Kim et al., 2016) Au NPs have been used in both SEECL sensors for ECL enhancement and ECL resonance energy transfer for ECL quenching. (Chen et al., 2017; Kuo et al., 2018; Zhang et al., 2018; Zhang et al., 2017) (iii) The PDA shell was employed to control the distance between QDs and Au NPs. PDA has superior biocompatibility and high specific surface area. And it has good thermodynamic stability and stable chemical properties on the electrode surface. In this experiment, the PDA shell was obtained by polymerizing dopamine. Because the ECL resonance energy transfer is a short-range effect, the increasing distance between the QDs and Au NPs by PDA shell can reduce the ECL resonance energy transfer effect largely. Furthermore, the low electrical conductivity of PDA also can help to limit electron transfer between QDs and Au NPs. Therefore, the obvious SEECL effect can be achieved with negligible resonance energy transfer. In the detection procedure of target p53 DNA, poly dimethyl diallyl ammonium chloride (PDDA) and poly (sodium-p-styrenesulfonate) (PSS) were modified on GCE to immobilize capture DNA. After capture DNA can hybridize with target DNA, the unreacted capture DNA hybridized with Au NPs@PDA@QDs nanocomposites-probe DNA. So the ECL signals of Au NPs@PDA@QDs nanocomposites decreased with the increase of the concentration of target DNA. The prepared biosensor was applied to the rapid detection of p53 gene in human blood with high selectivity, high sensitivity and high stability.

2. Experiment

2.1 Chemicals and reagents

All chemicals and reagents were of analytical grade and used directly without further purification. Copper (II) chloride dihydrate ($CuCl_2 \cdot 2H_2O$, 99.0%), indium chloride hydrate ($InCl_3 \cdot 4H_2O$, 99.9%), zinc chloride ($ZnCl_2$, 98.0%), sodium hydroxide (NaOH, 96.0%), thiourea ($CS(NH_2)_2$, 99.0%), mercaptopropionic acid (MPA) (99%), ethanol (99.7%), H_2SO_4 (98%) was purchased from HuaCheng Biological Co., Ltd (ChangChun). Sodium dihydrogen phosphate (NaH_2PO_4), disodium hydrogen phosphate (Na_2HPO_4) and sodium phosphate (Na_3PO_4) were purchased from Beijing Chemical Works. N-Ethyl-N‘-(3-dimethylaminopropyl) carbodiimide hydrochloride (EDC), N-hydroxysulfosuccinimide (NHS) and other materials were obtained from Beijing Dinggguo Chemicals Co. (Beijing, China). HAuCl4 was purchased from Acros Organics. All synthetic oligonucleotides were purchased from Sangon Biotech Co., Ltd. (Shanghai, China). The sequences of oligonucleotides were listed in Table S1. (Xu et al., 2017) All reagents were prepared using water with a resistivity of greater than 18 $M\Omega\ cm^{-1}$. Human serum was obtained as a gift from the school hospital, Jilin University. All experiments were carried out at room temperature.

2.2 Apparatus

Transmission electron microscopy (TEM) images were obtained with a Hitachi electron microscope operating at 200 kV acceleration voltages. Photoluminescence (PL) spectra measurements were performed on a Shimadzu RF-5301 PC spectrofluorophotometer (Shimadzu Co., Kyoto, Japan). The ultraviolet-visible (UV–vis) absorption spectra were acquired on a Varian GBC Cintra 10e UV–vis spectrometer with a 1 cm quart cell. All pH measurements were taken with a PHS-3C pH meter (Tuopu Co., Hangzhou, China). The electrochemical data were acquired with a CHI 660B electrochemical workstation with a three –electrode system. ECL signals were acquired by a BPCL ultraweak luminescence instrument. The voltage of the photomultiplier tube (PMT) was set at 900 V during the whole process. A conventional three-electrode system was used in this system. A glassy carbon

electrode (GCE) was used as the wording electrode. A platinum wire was employed as the counter electrode and an Ag/AgCl (saturated KCl) electrode as the reference electrode. In the ECL characterization experiments, the bare GCE was polished into a smooth interface by using 1.0 and 0.05 μm α-Al_2O_3 powder on rough paper. The polymelamine (pMel)/ GCE was prepared by electro-polymerization. In the electro-polymerization process, GCE was immersed in 0.1 mol/L H_2SO_4 containing 1.0 mmol/L melamine with the potential range of 0 to 1.6 V for 20 cycles. (Liu et al., 2012) As a result, GCE can be coated by pMel layer. Then QDs or Au NPs@PDA@QDs nanocomposites was dropped on the pMel/GCE for further experiments.

2.3 Synthesis of CuInZnS QDs and Quantum Yield (QY) Measurements

CuInZnS QDs were synthesized by hydrothermal method. $CuCl_2{\cdot}2H_2O$, $InCl_3{\cdot}4H_2O$ and $ZnCl_2$ solution were added in the conical flask separately. Then, the distilled water was added in the conical flask with MPA added into the solution and the solution became turbid to produce yellow particles. The pH of the mixture was adjusted to 11.3 by adding to 4 mol/L sodium hydroxide with stirring for 10 minutes. $CS(NH_2)_2$ solid was mixed in the system and the mixture became pale pink after dissolving. The above solution was transferred into a Teflon-lined stainless-steel autoclave. The autoclave was placed in the oven for 5 hours at a temperature of 180 ^oC. The molar ratio of $CuCl_2{\cdot}2H_2O$, $InCl_3{\cdot}4H_2O$ and $ZnCl_2$ was 3:10:5. The quantum yield of CuInZnS QDs was 6%. The QY of the CuInZnS QDs samples were measured according to the reported quantum yield of Rhodamine 6G.

2.4 Synthesis of Au NPs@PDA@QDs nanocomposites

AuNPs with average diameter about 19 nm were synthesized by the citrate-reduction method. 150 μL 0.1 g/mL $HAuCl_4$ and 150 mL water were added into three-neck flask with stirring vigorously and the three-neck flask was heated to boiling under reflux. Then 7.5 mL sodium citrate was added in the system quickly. When the solution was turned from yellow to deep red, the reaction was over. Then the solution was cooled to room temperature and stored at 4 ^oC in the refrigerator for

further use. Then, 1 mL Au NPs were added in 20 mL 2 mg/L dopamine Tris solution under stirring and allowed to proceed for 6 hours at room temperature. The PDA shell was obtained by polymerizing dopamine at room temperature. Dopamine was polymerized to PDA in pH 8.5, 10 mmol Tris-HCl buffer solution. The solution was separated by centrifuging and washed three times with distilled water. At the last step, 400 μL CuInZnS QDs, 700μL Au NPs@PDA and 900 μL distilled water were mixed together and shocked 30 minutes to obtain Au NPs@PDA@QDs nanocomposites.

2.5 Synthesis of Au NPs@PDA@QDs-probe DNA

Au NPs@PDA@QDs-probe DNA conjugates were prepared by covalent link carboxyl and amino. (Ai et al., 2012) 30 μL 10 mmol/L EDC and 10 μL 10 mmol/L NHS were added into as-prepared 2 mL Au NPs@PDA@QDs solution to activate carboxyl of CuInZnS QDs with stirring for 15 minutes. Then, 15 μL 10 μmol/L probe DNA was added and stirred for 2 hours. Finally, the solution was dialysed for 3 hours to remove the unreacted small molecules. Next, the Au NPs@PDA@QDs-probe DNA conjugates were preserved in a refrigerator at 4 ^{o}C for following experiment.

2.6 ECL detection

The bare GCE was polished into a smooth interface by using 1.0 and 0.05 μm α-Al_2O_3 powder on rough paper. The cleaned electrode was soaked in PDDA solution and PSS solution respectively for 5 minutes. Next, 10 μmol/L capture DNA was dropped onto PSS/PDDA/GCE and kept at room temperature. The capture DNA/PSS/PDDA/GCE was connected with target DNA at 70 ^{o}C for 5 minutes and cooled to room temperature. After hybridization, the electrode was washed with buffer solution (10 mmol/L Tris-HCl) and dried in air. Then, target DNA/capture DNA/PSS/PDDA/GCE was connected with Au NPs@PDA@QDs-probe DNA at 70 ^{o}C for 5 minutes and cooled to room temperature. After hybridization, the electrode was washed with buffer solution (10 mmol/L Tris-HCl). Next, Au NPs@PDA@QDs-probe DNA/ target DNA/capture DNA/PSS/PDDA/GCE was soaked in the bovine serum albumin (BSA) solution for 5 minutes, after which it was

rinsed with a buffer solution (10 mmol/L Tris-HCl).

For the measure of target DNA, the obtained Au NPs@PDA@QDs-probe DNA/ target DNA/capture DNA/PSS/PDDA/GCE ECL DNA biosensor was immersed in 0.1 mol/L phosphate buffer solution (pH=7.4) containing 0.1 mol/L $K_2S_2O_8$ as coreactant to record the ECL intensity. The ECL signal was collected in the coreactant under cyclic voltammetry from 0 to -2.5V.

2.7 Real Sample detection

Human serum was obtained as a gift from the school hospital, Jilin University. Samples were centrifuged at 10,000 rpm for 10 minutes to separate. 1.0 mL aliquot of serum sample was mixed with 1.5 mL acetonitrile. After shaking for 2 minutes, the solution was centrifuged at 10000 rpm for 10 minutes. The supernatant was adjusted to pH 7.4 with phosphate buffer solution. Different concentration of target DNA was added to the diluted serum samples to prepare the spiked samples.

3. Results and discussion

3.1 Characterization

Figure 1 showed the TEM image of (A) CuInZnS QDs, (B) Au NPs, (C) Au NPs@PDA and (D) Au NPs@PDA@QDs nanocomposites. The size of CuInZnS QDs was ca. 6 nm, and Au NPs had about 19 nm size. Both NPs were monodispersed well. The size of Au NPs@PDA was ca. 63 nm. It can be observed that Au NPs were encapsulated in the core of the Au NPs@PDA NPs. From the high-resolution TEM photo in Figure 1 (D), the structure of the Au NPs@PDA@QDs nanocomposites can be observed. The bright and dark areas were caused by the difference orientation in the sample structure. CuInZnS QDs were evenly distributed outside the Au NPs@PDA nanocomposites (as shown in the red ring). Figure S1 showed the EDX spectrum of the CuInZnS QDs, which proved that the composites contained Cu,In,Zn and S. This proved that CuInZnS QDs have been successfully synthesized. As is shown in Figure S2, the XRD pattern of the CuInZnS QDs revealed three

characteristic peaks at ca.27.2°, 62.3° and 77.2° corresponding to the (1 1 1), (2 2 0), and (3 1 1) ,which reflected that CuInZnS QDs was zinc blende type crystal. The PL emission spectrum of CuInZnS QDs was shown in Figure S3. The PL emission peak of CuInZnS QDs was at 568 nm. And the excitation peak was at 510 nm. As is shown in the Figure S4, the UV absorption peak of the Au NPs@PDA@QDs was at 406 nm and the UV absorption peak of QDs was at 418 nm, which had a blue shift of 12nm. Compared with QDs, Au@PDA@QDs nanocomposites possessed a large amount of $-NH_2$. The electron affinity of the N atom in $-NH_2$ was relatively strong, which resulted in the occurrence of n-π* transitions. So, the absorption peak of Au NPs@PDA@QDs nanocomposites had blue shift. (Ju et al., 2014; Qu et al., 2013) And it also confirmed that the Au NPs@PDA@QDs nanocomposites has been synthesized successfully.

Figure S5 illustrated the cyclic voltammograms of Au NPs@PDA@QDs nanocomposites, Au NPs@PDA nanocomposites and CuInZnS QDs. Au NPs@PDA nanocomposites had an oxidation peak. This was due to a large number of reducing groups ($–NH_2$) were oxidized on the surface of Au NPs@PDA nanocomposites. Compared with CuInZnS QDs, Au NPs@PDA@QDs nanocomposites had a larger reduction current peak. It was due to the surface oxygen groups were reduced and the large surface area of the PDA. As a result, more QDs can be bound on the surface of PDA shell. The cathode current peak became large. And compared with the cyclic voltammograms of Au NPs@PDA nanocomposites, it is also confirmed that Au NPs@PDA@QDs nanocomposites were successfully synthesized.

3.2 Condition optimization

To achieve the high-performance ECL signal, the effect of $K_2S_2O_8$ concentration, pH value and scan rate on the ECL intensity of Au NPs@PDA@QDs nanocomposites were investigated (Figure S6). $K_2S_2O_8$ worked as co-reactant in ECL. With the increased concentration of co-reactant, the ECL intensity was enhanced. And the ECL

intensity reached a maximum at 0.09 mol/L $K_2S_2O_8$. More co-reactant with consequent excessive amount of SO_4^{2-} can suppress the reaction to produce excited state QDs and resulted into the ECL intensity quenching. In order to investigate the suppressing effect of SO_4^{2-} concentration, we added 0.01 mol/L-0.05 mol/L SO_4^{2-} in 0.1 mol/L $K_2S_2O_8$ as co-reactant respectively to detect the ECL intensity of QDs (shown in Fig.S6 D). The ECL quenching results confirmed that SO_4^{2-} can suppress the reaction to produce excited state QDs.

The pH value also had a great effect on ECL. The ECL intensity reached its maximum at pH 6. The ECL behavior of the sensor system depended largely on the rate of generation of excited-state QDs. When the scan rate was below 0.2 V/s, the ECL intensity increased with the scan rate increasing and reached the maximum at 0.2 V/s. This was due to the formation of more excited-state QDs within short time span. The high scan rate can enrich excited-state QDs within short time span and increase ECL intensity. While the scan rate was over 0.2 V/s, the ECL intensity decreased because the electrochemical process was irreversible. (Liu et al., 2015)

3.3 EIS and ECL behavior of the nanocomposites

Electrochemical impedance spectroscopy (EIS) was used to describe the change of impedance during the process of electrode modification. The semicircle diameter at higher frequencies represented the resistance of electron transfer, and the linear part at lower frequencies represented the diffusion process. (Liu et al., 2016) As shown in Figure S7, the cleaned GCE showed a mass diffusion limiting process. (Liang et al., 2014) The electron-transfer resistance increased to 201.7 Ω with the modification of melamine (Mel) and QDs on GCE (QDs/Mel/GCE). And the electron-tranfer resistance increased to 221.4 Ω with the modification of Mel and Au NPs@PDA@QDs

nanocomposites on GCE. There was not much impedance difference between QDs and Au NPs@PDA@QDs nanocomposites, which also confirmed that PDA successfully blocked the electron transfer between Au NPs and QDs.

In the prepared ECL system, the ECL behavior of Au NPs@PDA@QDs nanocomposites was caused by the reaction between luminescent CuInZnS QDs and co-reactant $S_2O_8^{2-}$, and Au NPs could enhance the ECL intensity of QDs. With the potential scanning from -2.5 V to 0 V, both QDs and $S_2O_8^{2-}$ were reduced $QDs^{\cdot-}$ and $SO_4^{\cdot-}$, respectively. Then, $QDs^{\cdot-}$ and $SO_4^{\cdot-}$ got together quickly and produced the excited state CuInZnS QDs*. The ECL intensity could be detected when the excited state CuInZnS QDs* returned to the ground state with the existence of the $K_2S_2O_8$ co-reactant. The mechanism for ECL generation is according to the equations below:

$$\text{CuInZnS QDs} + e^- \rightarrow \text{CuInZnS QDs}^{\cdot-} \quad (1)$$

$$S_2O_8^{2-} + e^- \rightarrow SO_4^{2-} + SO_4^{\cdot-} \quad (2)$$

$$\text{CuInZnS QDs}^{\cdot-} + SO_4^{\cdot-} \rightarrow \text{CuInZnS QDs*} + SO_4^{2-} \quad (3)$$

$$\text{CuInZnS QDs*} \rightarrow \text{CuInZnS QDs} + h\nu \quad (4)$$

It can be seen from Figure 2 (A) that both QDs and Au NPs@PDA@QDs nanocomposites had the biggest ECL signals at the -2.5V. The ECL signal of Au NPs@PDA@QDs nanocomposites was twice as much as the ECL signal of QDs because of the SPR effect. As shown in Figure S8 and Figure 2 (B), the introduction of Au NPs increased the PL intensity due to the SPR effect. The ECL intensity of QDs, QDs/Au NPs, QDs@PDA, QDs@PDA@Au NPs were also discussed to show different SPR effect on QDs ECL. Only the ECL intensity of Au NPs@PDA@QDs nanocomposites was enhanced largely. It indicated that the PDA shell and sensor structure were critical factor in SEECL system. The PDA shell provided an ideal distance between Au NPs and QDs without electron transfer.

3.4 ECL response to p53 gene

As was shown in Figure 3, the ECL intensity of Au NPs@PDA@QDs nanocomposites decreased with the concentration of target DNA increasing. The linear relation between the ECL intensity and the concentration of target DNA was shown in Figure 3 (A). The linear range was from 0.1 nmol/L to 15 nmol/L. When the concentration of p53 gene was in the range of 0.1 nmol/L to 3.57 nmol/L, the linear equation was Y=-0.20X+5.45 with the squared correlation coefficient of 0.96. (Y represented lg ECL intensity and X represented the concentration of p53 gene) And the linear equation was Y=-0.01X+4.78 with the squared correlation coefficient of 0.93 for 3.57~15 nmol/L p53 gene. The limit of detection (LOD) was determined as 0.03 nmol/L, which was referred to LOD $=3S_B/m$ (S_B was the standard deviation of the blank, and m was the slope of the corresponding calibration curve) (Singla et al., 2014).

The stability of the proposed Au NPs@PDA@QDs nanocomposites on GCE (Figure S9) was evaluated by successive measurements (n=19) in phosphate buffer solution (pH=7.4) containing 0.09 mol/L $K_2S_2O_8$. The relative standard deviation (RSD) was 3.38%. It indicated that the outstanding stability of Au NPs@PDA@QDs nanocomposites on GCE. This satisfactory result showed that Au NPs@PDA@QDs had a very wide range of applications.

In order to investigate the selectivity of the ECL biosensor, one-base-mismatched DNA was employed. Figure 4 showed the ECL intensity change in the presence of complementary target DNA and one-base-mismatched DNA. $\Delta I = I-I_0$, I and I_0 referred to the ECL intensity of ECL sensor in the presence and absence of target DNA or one-base-mismatched DNA, respectively. The ECL intensity ratio was obtained with the addition of 1 nmol/L target DNA and one-base-mismatched DNA. The $\Delta I/I_0$ value obtained on the addition of one-base mismatched DNA p53 was approximately 7%, while the value obtained on the addition of the same concentration of complementary target DNA was 38.35%. This result indicated the sensor had good and acceptable selectivity, which was in accord with the previous similar reports (Sharma et al., 2018, Bizid et al., 2018). The RSD were

2.32% and 4.5% respectively. We compared some methods for detecting the p53 gene as shown in Table S2. The proposed ECL biosensor also showed good sensitivity.

3.6 Detection of p53 gene in real samples

In order to evaluate the feasibility of this sensing system, a series of samples spiking target DNA in human serum were detected. The results were listed in Table 1. The recoveries were in the range of 88%~103.4% and the RSD was less than 2.52%, indicating that the results indicated that the accuracy and precision of the proposed method were satisfactory.

4. Conclusion

The research provided the characterisation and expansion of a novel SEECL DNA sensor for p53 gene detection based on CuInZnS QDs and Au NPs. PDA shell controlled the separation length between Au NPs and QDs to induce SPR enhanced ECL response. Moreover, PDA can also successfully block the electron transfer between Au NPs and CuInZnS QDs. The p53 gene had a superior linear response (0.1 nmol/L-15 nmol/L) with $K_2S_2O_8$ as a co-reactant. The DNA sensor had good stability and sensitivity. And we will regard the selectivity of SEECL DNA sensor as our focus in the future. The new type of SEECL sensor has great potential for future biological application and diagnostics.

Acknowledgements

The authors gratefully acknowledge financial support from the National Natural Science Foundation of China (No 21005029), Youth Science Fund of Jilin Province (No 20140520081JH) and “Thirteenth Five Year” Project of the Science and Technology Research in the Education Department of Jilin Province, China (No JJKH20180125KJ)

References

Ai X. Z., Niu L., Li Y. Y., Yang F. P., Su X. G., 2012, Talanta 99**,** 409-414.

Bizid S., Blili S., Milka R., Said A. J., Korri-Youssoufi H., 2018, Talanta, 184, 475-483.

Chen S. F., Chen X. Q., Xia T. T., Ma Q., 2016, Biosens. Bioelectron., 85, 903-908.

Chen X. Q., Gui W. Y., Liu H. and Ma Q., 2017, Analyst, 142**,** 4142

Chen X. Q., Gui W. Y. and Ma Q., 2018, Anal. Chim. Acta. 1009, 73-80.

Chen X. Q., Liu Y. and Ma Q., 2018, J. Mater. Chem. C, 6, 942-959.

Chen Z. P., Xie C. P., Yang F., Feng L. and Xiang W. D., 2014. J. Alloys Comp., 594, 107-113.

Jiang W. T., Liu L., Chen Y., 2018, Anal. Chem., 5, 3058-3066

Ju J., Zhang R. Z., He S. J. and Chen W., 2014, RSC. Adv., 4, 52583

Khoshfetrat S. M., Bagheri H., Mehrgardi M. A. 2018, Biosens. Bioelectron., 100, 382-388.

Kim J. E., Choi J. H., Colas M., Kim D. H. and Lee H., 2016, Biosens. Bioelectron., 80, 543-559.

Kuo P.C., Lien C. W., Mao J. Y., Unnikrishnan B., Chang H.T., Lin H. J. and Huang C. C., 2018, Anal. Chim. Acta. 1009, 89-97.

Le Q. L. and Ding S. N., 2016. Sci. Bull., 61 (12), 931-938.

Liang H., Song D. D., Gong J. M., 2014, Biosens. Bioelectron. 53**,** 363-369.

Lin X. Y., Xu S. H., Wang C. L., Wang Z. Y. and Cui Y. P., 2014. RSC Adv, 4, 4993.

Liu L. L., Ma Q., Li Y., Liu Z. P., Su X. G., 2015, Biosens. Bioelectron., 63, 519-524.

Liu L. L., Wang X. Y., Ma Q., Lin Z. H., Chen S. F., Li Y., Lu L. H., Qu H. P. and Su X. G., 2016, Anal. Chim. Acta., 916, 92-101

Liu X., Luo L., Ding Y., Wu Q., Wei Y., Ye D., 2012, J. Electroanal. Chem. 675**,** 47-53

Milicevic Z., Bajic V., Zivkovic L., Kasapovic J., Andjelkovic U., Spremo-Potparevic B., 2014, Sci. World J. 2014, 618698.

Qu D., Zheng M., Du P., Zhou Y., Zhang L. G., Li D., Tan H. Q., Zhao Z., Xie Z. G. and Sun Z. C., 2013, Nanoscale, 5, 12272

Sharma D., Lee J., Shin H., 2018, Biosens. Bioelectron., 107, 10-16.

Singla P., Kaur P., Singh K., 2014, Talanta, 571-576

Tendler Y., Weisinger G., Coleman R., Diamond E., Lischinsky S., Kerner H., Rotter V., Zinder O., 1999, Mol. Brain Res, 72, 40-46.

Wang C. L., Xu S. H., Shao Y. J., Wang Z. Y., Xu Q. Y. and Cui Y. P., 2014. J. Mater. Chem. C, 2, 5111.

Wang J., Shan Y., Zhao W., Xu J. and Chen H., 2011, Anal. Chem., 83, 4004–4011.

Wu L., Ding F., Yin W. M., Ma J., Wang B., Nie A., Han H. Y., 2017. Anal. Chem. 89, 7578-7585.

Xu H., Xue C., Zhang R. B., Chen Y. R., Li F., Shen Z. F., Jia L. and Wu Z. S., 2017, Sens. Actuators. B, 243, 1240-1247.

Yang Y. K., Fang G. Z., Wang X. M., Zhang F. Y., Liu J. M., Zheng W. J., Wang S., 2017, Electrochim. Acta, 228, 107-113.

Ye S. J., Ye R. H., Shi Y. D., Qiu B., Guo L. H., Huang D. H., Lin Z. Y., Chen G. N., 2017. Anal. Bioanal. Chem., 409, 7145-7151.

Zhang W., Xiong H. W., Chen M. M., Zhang X. H., Wang S. F., 2017. Biosens. Bioelectron. 96, 55-61.

Zhang X. B., Li Y. Y., Lv H., Feng J. H., Gao Z. Q., Wang P., Dong Y. H., Liu Q. and Zhao Z. D., 2018, Biosens. Bioelectron., 106, 142-148.

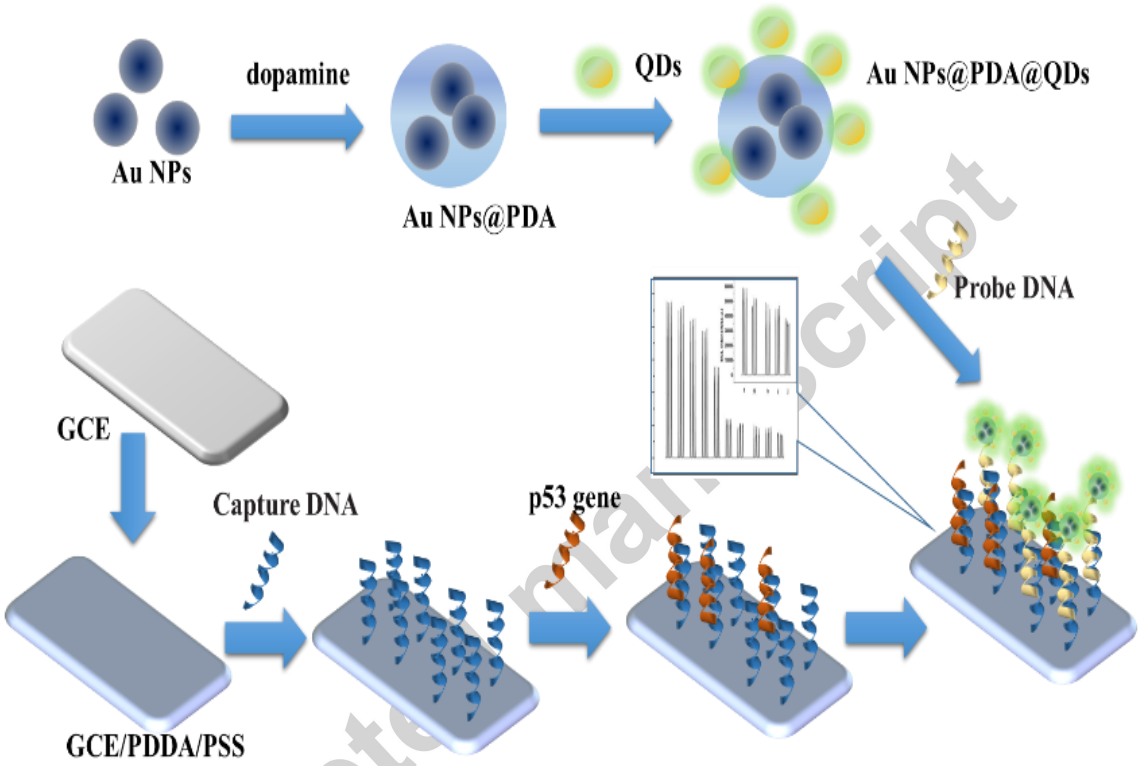

Scheme 1 The procedure of synthesizing Au NPs@PDA@QDs nanocomposites and the procedure of the detection of p53.

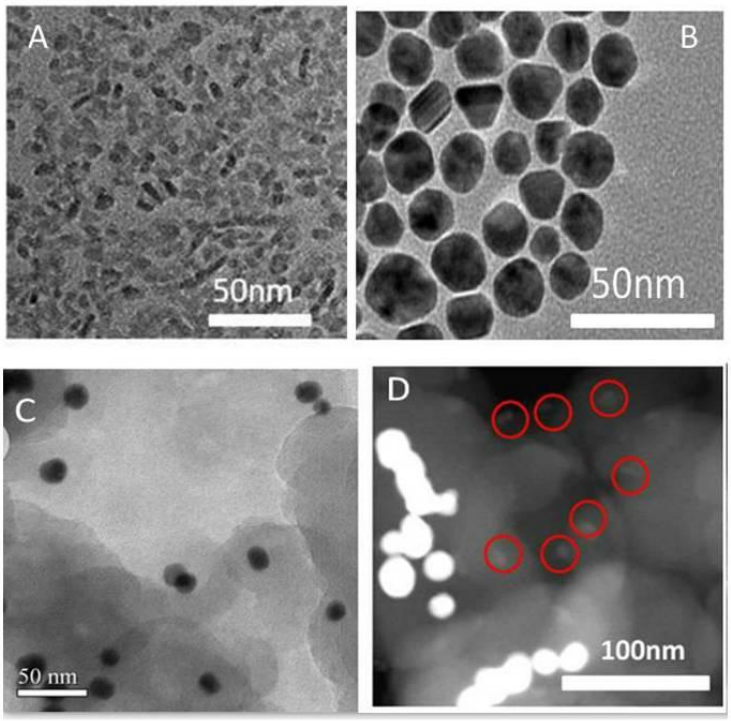

Figure 1 TEM photograph of (A) CuInZnS QDs (B) Au NPs (C) Au NPs@PDA NPs (D) Au NPs@PDA@QDs nanocomposites (HRTEM)

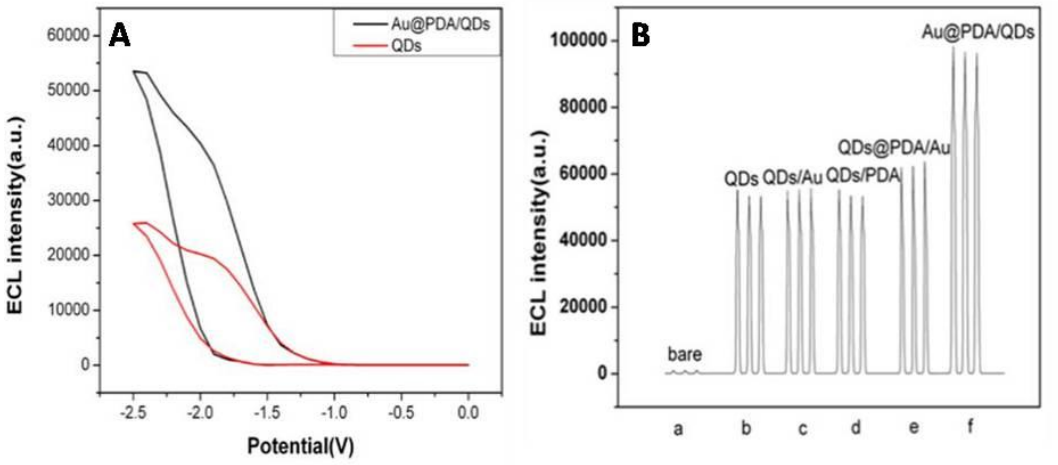

Figure 2 (A) ECL response of QDs and Au NPs@PDA@QDs nanocomposites. (B) ECL curves of (a) GCE (b) QDs (c) QDs@Au NPs (d) QDs@PDA (e) QDs@PDA@Au NPs (f) Au NPs@PDA@QDs.

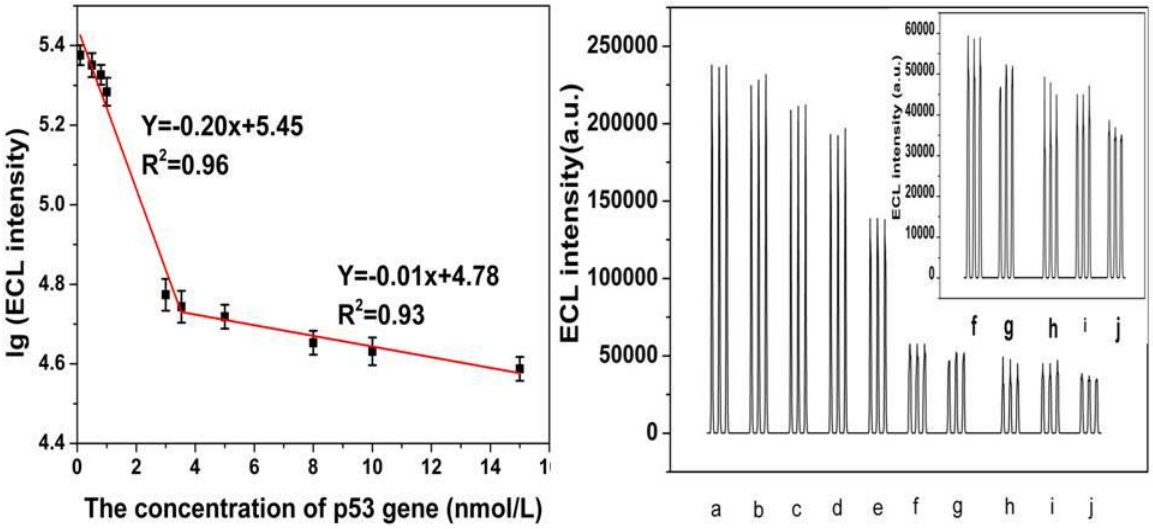

Figure 3 (A) The linear relation between the ECL intensity and the concentration of target DNA (B) ECL time trace of Au NPs@PDA@QDs nanocomposites -probe DNA/target DNA/capture DNA/PSS/PDDA/GCE to different of concentration of target DNA.

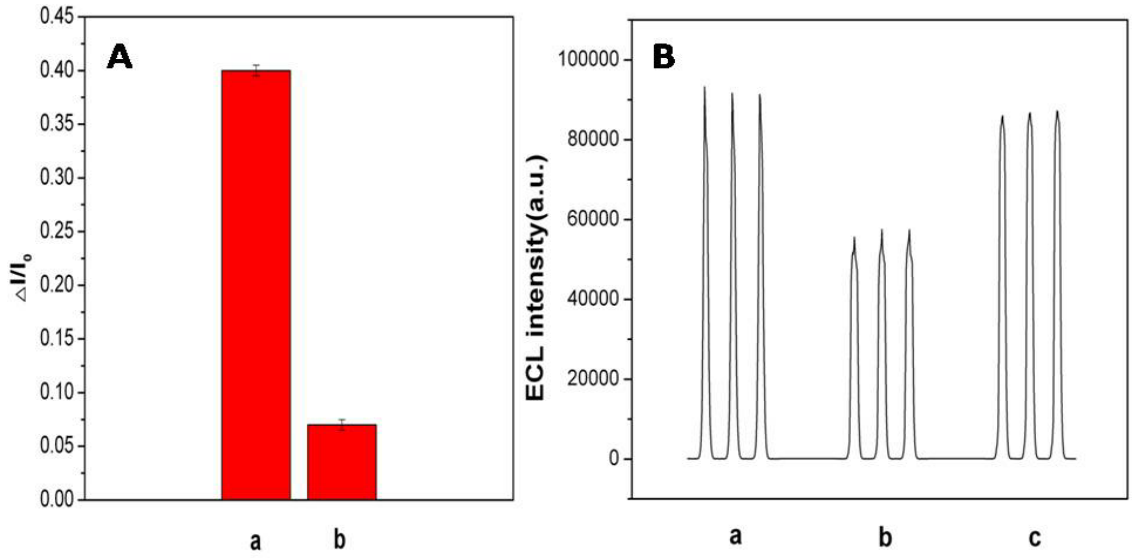

Figure 4 (A) The ECL intensity ratio $\Delta I / I_0$ ($\Delta I = I - I_0$) in the presence of (a) complementary target DNA, (b) one-base-mismatched DNA. (B) ECL-time curves of (a) blank sample, (b) complementary target DNA, (c) one-base-mismatched DNA.

Table 1 Results of determination of target DNA in human serum samples.

Sample	Spiked (nmol/L)	Founded (nmol/L)	Recovery (%)	RSD (%)
1	0.1	0.088	88.0	1.76
2	1	0.92	92.0	2.52
3	10	10.34	103.4	2.18

Highlights

- CuInZnS QDs are ideal luminophore for ECL sensing application. Compared with the traditional chalcogenide QDs, CuInZnS QDs have good biocompatibility and non-toxicity. Moreover, the luminescence of CuInZnS QDs is mainly due to surface defect state emission. So, the ECL emission of QDs depends on the surface states with high ECL efficiency.
- Au NPs in the core of the nanocomposite worked as ECL enhancer.
- The PDA shell was employed to control the distance between QDs and Au NPs.